CHEMISTRY
A EUROPEAN JOURNAL

DOI: 10.1002/chem.200600396

Experimental and Theoretical Investigations on the Catalytic Hydrosilylation of Carbon Dioxide with Ruthenium Nitrile Complexes

Peter Deglmann,*[b] Erika Ember,[c, d] Peter Hofmann,*[a] Stephan Pitter,*[c] and Olaf Walter[c]

Dedicated to Professor Dr. Dr. h.c. Rolf Gleiter on the occasion of his 70th birthday

Abstract: Ruthenium complexes, *mer*-$[RuX_3(MeCN)_3]$ and *cis*/*trans*-$[RuX_2(MeCN)_4]$ with X = Br, Cl, were investigated as precatalysts in homogeneously catalyzed hydrosilylation of CO_2. The oxidation state of ruthenium and nature of the halide in the precatalysts were found to influence the catalytic activity in the conversion of Me_2PhSiH to the formoxysilane $Me_2PhSiOCHO$, with Ru^{III} having chloride ligands being most active. Monitoring the reactions by in-situ IR spectroscopy in MeCN as the solvent indicates an interaction of the precatalyst with the silane prior to activation of CO_2. In the absence of CO_2, hydrosilylation of the MeCN solvent occurs. Catalytic activity in CO_2 hydrosilylation is enhanced by $Me_2PhSiCl$, generated during reduction of Ru^{III} in *mer*-$[RuX_3(MeCN)_3]$ to Ru^{II} or, when added as promoter to Ru^{II} precatalysts. The reaction mechanism for the catalytic cycle has been calculated by DFT methods for the reaction of Me_3SiH. The key steps are: Transfer of the Me_3Si moiety to a coordinated halide ligand, resulting in an $L_nRuH(XSiMe_3)$ intermediate → CO_2 coordination → Me_3Si transfer to CO_2 → reductive elimination of formoxysilane product. This reaction sequence is more favorable energetically for chloride complexes than for the analogous bromide complexes, which accounts for their differences in catalytic activity. Calculations also explain the rate increase observed experimentally in the presence of $Me_2PhSiCl$. A parallel reaction pathway leads to $(Me_3Si)_2O$ as a minor byproduct which arises from the condensation of two initially formed Me_3SiOH molecules.

Keywords: carbon dioxide fixation · homogeneous catalysis · hydrosilylation · ruthenium

Introduction

Silyl acetates $(MeCO_2)_mSiR_n$ are important building blocks in the production of silicones due to their ability to undergo condensations with a concomitant release of acetic acid.[1] The introduction of the leaving group requires an organic feedstock for the acetyl unit. Analogous formoxysilyl derivatives $(HCO_2)_mSiR_n$ are potential substitutes in polycondensation[2] and the release of formic acid due to its volatility and fungicidal action could also offer advantages in certain applications. Apart from organic esterification,[3] formoxysilanes can be synthesized by the homogeneously catalyzed hydrosilylation of CO_2, an approach which is fully efficient atomically if the formyl unit is introduced from CO_2. In 1981 both Koinuma et al. and Süss-Fink et al. reported a ruthenium catalyzed CO_2 hydrosilylation (Scheme 1).[4] Later, Jessop showed that this reaction is feasible also under solvent-less conditions in supercritical CO_2 ($scCO_2$) with the catalyst $[RuH_2(PMe_3)_4]$;[5] however, if competing with olefin hydrosilylation in $scCO_2$, conversion of CO_2 is not observed

[a] Prof. P. Hofmann
University of Heidelberg, Department of Organic Chemistry
INF 270, 69120 Heidelberg (Germany)
Fax: (+49) 6221-54-4885
E-mail: ph@oci.uni-heidelberg.de

[b] Dr. P. Deglmann
present address:
GKP/M, BASF AG, 67056 Ludwigshafen (Germany)
Fax: (+49) 621-609-9976
E-mail: peter.deglmann@basf.com

[c] Dr. E. Ember, Dr. S. Pitter, Dr. O. Walter
Karlsruhe Research Center, ITC-CPV, Molecular Catalysis
P.O. Box 3640, 76021 Karlsruhe (Germany)
Fax: (+49) 7247-82-2244
E-mail: stephan.pitter@itc-cpv.fzk.de

[d] Dr. E. Ember
present address:
University of Erlangen, Institute of Inorganic Chemistry,
Ergerlandstrasse 1, 91058 Erlangen (Germany)
Fax: (+49) 621-609-9976

Supporting information for this article is available on the WWW under http://www.chemeurj.org/ or from the author: Details of the structural analyses of complexes **7** and **10** previously not reported.

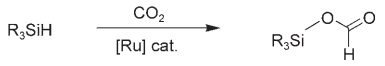

Scheme 1. CO_2 Hydrosilylation.

for $[RuCl_2\{P(C_6H_4\text{-}p\text{-}CF_3)_3\}_3]$,[6] or for Karstedt's Pt catalyst.[7] Moreover, non-catalyzed CO_2 insertion into the Si–H bond of a hypervalent organosilane is also known.[8]

Employing simple ruthenium complexes as catalysts, we recently showed that various tertiary and secondary silanes undergo CO_2 hydrosilylation with Si–O bond formation.[9] Disiloxanes are the only byproducts observed in significant amounts, while further reduction of formoxysilane products does not take place, contrary to the case of iridium catalysis.[10]

Although we have since discovered catalysts of enhanced activity, and have also developed an approach for catalyst recycling,[11] the mechanism of the CO_2 hydrosilylation is not yet understood in detail. Our earlier investigations revealed that probably Ru^{II} formed by reduction of Ru^{III} precatalysts initiate the catalytic cycle.[9a] Eisenberg et al. studied the reversible addition of Me_3SiH to CO_2, catalyzed by [Ir(CN)(CO)dppe], by NMR techniques to show the presence of various iridium hydride complexes.[10] Süss-Fink et al. proposed silyl group transfer to the active site as the step initiating the catalytic cycle when starting from ruthenium cluster anions as precatalysts (Scheme 2).[4b]

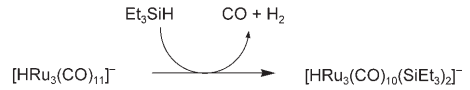

Scheme 2. Formation of the active catalyst in CO_2 hydrosilylation proposed by Süss-Fink et al.

On the other hand, mechanism of alkene hydrosilylation has been studied extensively.[12,13] Two pathways (Scheme 3), differing in hydride or silyl group transfer are the Chalk-Harrod (a)[14] and the modified Chalk-Harrod (b) mechanism, respectively.[15] Hydrogenation of CO_2, for which also pathways with different orders of substrate activation have been proposed, depending on the catalyst and, more importantly, on the solvent, is another related reaction.[16] One common feature of olefin hydrosilylation and CO_2 hydrogenation is the prior interaction of the reducing substrate, H_2 or R_3SiH, with the metal center of the catalyst.

This report gives an account on new developments in the CO_2 hydrosilylation, leading to improved reactivity, and proposes a mechanism based on latest experimental and DFT studies.

Results and Discussion

Precatalysts: Mixed halide nitrile complexes of ruthenium

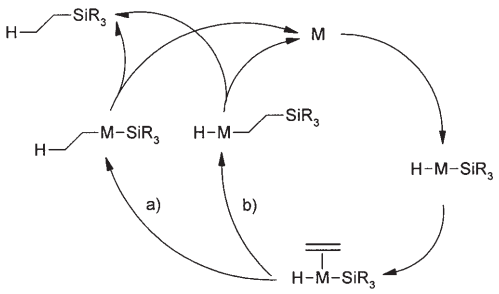

Scheme 3. Chalk–Harrod (a) and modified Chalk–Harrod (b) hydrosilylation mechanism.

were studied in the past particularly with respect to their redox properties.[17] Also, their use in designing antitumor agents was reported.[18] Catalytic reactions directly employing $L_nRuX_x(RCN)_y$ complexes have not been reported so far, whereas *mer*-$[RuCl_3(MeCN)_3]$ (**5**) has been used as an electron transfer mediator in the electrocatalytic oxidation of cyclic olefins.[17a] Also, Ru^{II} complexes with labile bonded MeCN ligands were studied as precursors of homogeneous hydrogenation catalysts.[19]

Reducing $RuCl_3{\cdot}n\,H_2O$ (**1**) with silanes in MeCN at 358 K afforded high yields of $[Ru^{II}Cl(MeCN)_5][trans\text{-}Ru^{III}Cl_4(MeCN)_2]$ (**11**) which was found to be an excellent catalyst for the CO_2 hydrosilylation.[9a] Despite the excess of silane present in the reaction, half the ruthenium stays in its former oxidation state (+3), probably because complex **11** is insoluble. Because in complex **11** the anion and cation are different in both coordination sphere and oxidation state, we decided to study neutral ruthenium complexes to investigate in more detail the precatalysts effects. Complexes of the $[RuX_2(MeCN)_4]$ and $[RuX_3(MeCN)_3]$ types seemed to be promising precursors. In a previous investigation we also demonstrated that the catalyst derived from complex **11** is easy to recycle.[11]

Heating of $RuCl_3{\cdot}n\,H_2O$ (**1**) or $RuBr_3{\cdot}n\,H_2O$ (**2**) in nitrile solution affords complexes of the type *mer*-$[RuX_3(RCN)_3]$ (Scheme 4).[20]

At elevated temperatures yields are 94% for complex **5** and 83% for complex **6**. Intense refluxing of the reaction solution increases byproduct formation (see preparation of **5** and **6**, Experimental Section). An analogous complexation attempt in order to obtain $[RuI_3(RCN)_3]$ from RuI_3 failed.

Reduction of complexes **5** and **6** allows for controlled synthesis of neutral complexes $[Ru^{II}X_2(MeCN)_4]$ (Scheme 4). Other methods of their preparation are also known: *trans*-$[Ru^{II}Cl_2(MeCN)_4]$ (**9**) was synthesized by photo-induced

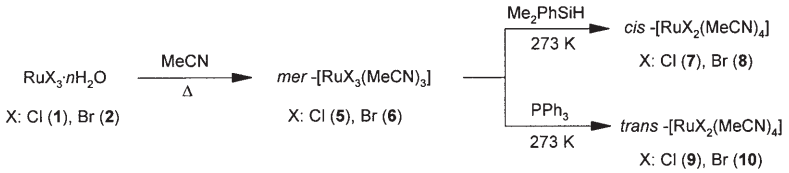

Scheme 4. Synthesis of ruthenium complexes.

ligand exchange from $[Ru^{II}Cl_2(o\text{-}Bu_2C_6H_4)]$ and its structure characterized;[21] its synthesis was also reported starting from $RuCl_3{\cdot}n\,H_2O$ via H_2 reduction in MeCN.[22] We found the reduction of **5** and **6** with silanes to afford selectively the *cis*-isomers of $[Ru^{II}X_2(MeCN)_4]$ (**7**: X = Cl; **8**: X = Br). Unlike the synthesis of complex **11**, as outlined above, crystallization is slow and therefore Ru^{III} is reduced completely to Ru^{II}. Phosphine reduction allows for synthesis of the corresponding *trans*-isomers of $[Ru^{II}X_2(MeCN)_4]$ (**9**: X = Cl); **10**: X = Br) (Scheme 4). No phosphine complexation at the ruthenium center by replacement of MeCN ligands was observed, the isolated yields of complexes **9** and **10** being similar to those of complexes **7** and **8**, respectively. All neutral ruthenium complexes **5** to **10** are sufficiently soluble in MeCN at room temperature within the concentration range required for CO_2 hydrosilylation, typically between 1 and 20 mmol L^{-1}. As outlined above, the ionic complex **11** dissolves in MeCN only at a higher temperature.

In the solid state, all complexes **5** to **10** show positive IR shifts for the C–N stretching frequency of the coordinated MeCN ligands compared with free MeCN (2254 cm^{-1}), which supports the assumption that backbonding from ruthenium to MeCN is negligible (Table 1). Absorptions at 2321 cm^{-1} (**5**) and 2327 cm^{-1} (**6**) result from combination of the symmetrical CH_3 deformation and the C–C stretching.[23]

The ^1H NMR data of the *mer*-complexes **5** and **6** (Table 1), which have not yet been reported, show paramagnetic shifts for the coordinated MeCN ligands as expected for Ru^{III}. The Ru^{II} complexes show two resonances for the *cis*-isomer **7** and one resonance for each *trans*-isomer (**9** and **10**). The *cis*-isomer **8** shows only one resonance for both pairs of methyl protons. Dynamic effects including the potential exchange of weakly coordinating MeCN or halide dissociation were considered by variable temperature measurements of a mixture of **7** and **8** in CD_3CN. It turned out that exchange of coordinated MeCN takes place at temperature above 330 K, faster for the *cis*-isomer **7** than for the *trans*-isomer **8**. At temperature below, down to 240 K, no dynamic effects are observed.

In situ monitoring of CO_2 hydrosilylation by FTIR spectroscopy: The stability of operating conditions with the ReactIR 1000 system was checked in preliminary experiments to detect potential effects of heating, pressurization, and agitation on absorption intensities and frequencies. The DiComp probe employed in this study offers very stable conditions throughout the complete reaction period. There are two main points to be considered when setting up the experimental conditions. On the one hand, the refractive index of the reaction medium changes during the reaction, in particular at higher substrate concentrations. On the other hand, the spectral baseline usually shifts upward during heating. No shifts in the absorption frequencies were observed under these conditions. From among the different quantification techniques applicable for such measurements (QuantIR software package, peak area analysis, peak height analysis), the peak height analysis was chosen.

Figure 1 shows the representative stacked plot of a complete reaction course monitored. Apart from the Si–H stretching frequency, where the diamond probe has its absorption, all major vibrations of silane **3** and the product **4** were observed. Characteristic absorptions are labeled which can be used to calculate the concentrations of both silane **3** and $Me_2PhSiOCHO$ (**4**). The data given here are based on the consumption of silane **3** as monitored by its Si–H wagging vibration at 885 cm^{-1} (**A**). As the hydrosilylation approach described here offers excellent product selectivity, alternatively also the carbonyl stretching frequency of formoxysilane **4** at 1710 cm^{-1} (**B**) could be used; however; its intensity usually is lower and, in particular, the data for low product concentrations do not allow for initial reaction rates to be determined. The kinetic data presented below, and their corresponding concentra-

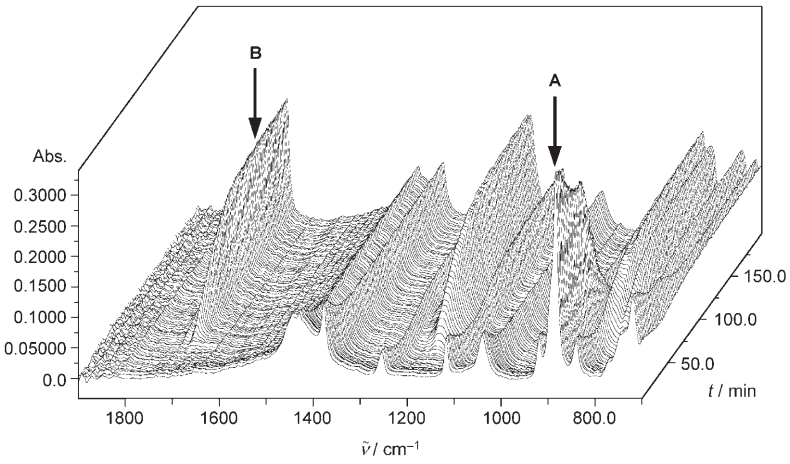

Figure 1. Representative plot of IR spectra versus time for the CO_2 hydrosilylation.

Table 1. Selected spectroscopic data of complexes **5**–**10**.

	5	**6**	**7**	**8**	**9**	**10**
region ν_{CN} [cm^{-1}]	2294, 2321	2289, 2327	2276	2277	2279	2279
^1H NMR [ppm]	−15.6 (s, ~6H)	−14.9 (s, ~6H)	2.50 (s, 3H)	2.54 (s)	2.54 (br s)	2.54 (s)
	47.8 (s, ~3H)	39.4 (s, ~3H)	2.51 (s, 3H)			

tion levels were validated in representative experiments by off-line analyses of samples taken from reaction mixtures. The experiments were performed to clarify three distinct influence factors, that is, the oxidation state of the precatalyst, the kind of halide ligand coordinated at the metal center, and the order of silane and CO_2 dosing. The results are summarized in Tables 2 and 3.

Table 2 summarizes the results for the case when all components are introduced into the reactor prior to heating. In all experiments 1–6, a significant induction period was observed before the catalyst reached its maximum activity. Silane conversion is high in all experiments, and product selectivity in formoxysilane **4** is between 82 and 99%. The byproducts are the same as those stated in previous reports: $Me_2PhSiOSiMe_2Ph$ and Me_2PhSiX (traces; X: Cl, Br).[9a]

Table 2. Hydrosilylation of CO_2 by using Method A (all substances were introduced at 25 °C).[a]

Entry	Precatalyst[b]	Induction [min]	TOF [h^{-1}][c]	Conversion (%)[d]	Yield [%][d]	Selectivity [%][d]
1	**5**	19	390	> 99	> 99	> 99
2	**6**	41	190	85	81	95
3	**7**	47	260	100	> 99	> 99
4	**8**	144	190	83	81	98
5	**9**	78	140	> 99	82	82
6	**10**	n.d.[e]	40	87	73	84

[a] Conditions (see Experimental Section): 20 mL MeCN, 20 mmol Me_2PhSiH (**3**); T = 358 K. [b] 40 μmol. [c] Turn-over-frequency: [mol silane **6**]/[mol Ru][t]; based on yields given in the table and calculated from the period when product formation was measured. [d] Values are based on ^1H NMR analysis of the product solution. [e] Due to the low activity of complex **10**, the induction period cannot be distinguished from the reaction.

There is clear experimental evidence to show that chloride ligands improve activity, expressed by the TOF value, compared to the respective bromide complexes (entries 1–2, 3–4, 5–6). Similar iodide complexes, such as $[Ru^{II}I(MeCN)_5]I{\cdot}MeCN$ were found to be catalytically inactive and, therefore, were not taken into account in further studies.[24]

Although it might be assumed that the reduction potential of the silane favors conversion of Ru^{III} to Ru^{II}, which then should be the oxidation state of the active catalyst in any case, the Ru^{III} precatalysts generally exhibit even higher activities (entries 1,2) than their Ru^{II} counterparts (entries 3 to 6).

Figure 2 illustrates a representative full reaction (entry 2) as a function of concentrations (calculated from IR absorption intensities) plotted versus time and temperature. Note that the results, as indicated in Table 2, are corrected for shifts in absorbances caused by heating (0–40 min). It is remarkable that, although the final temperature is reached in approximately 40 min, product formation starts in 100 min and, as shown in Table 2, maximum activity of the catalyst generally is obtained only after a certain induction period depending on the precatalyst used. This is believed to be related to the pre-activation of the catalyst. An intermediate absorption at 1676 cm^{-1} was observed during this pre-activation, indicating a preceding unknown reaction. Therefore, entries 1 to 6 (Table 2) were repeated under different experimental conditions where CO_2 was added 15 min after the reaction temperature had been reached (Method B). The acceleration effect is shown in Figure 3 (entry 2, Table 3),

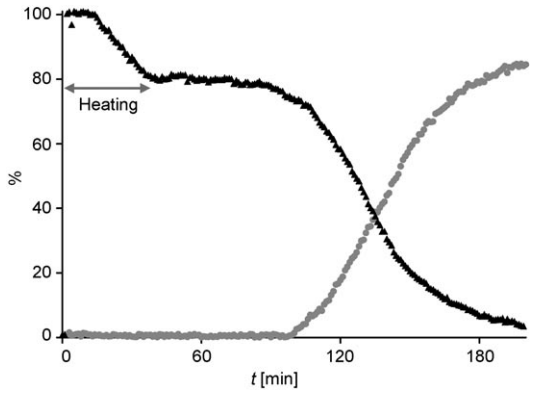

Figure 2. Conversion of silane **3** (▲) and formation of formoxysilane **4** (●) plotted versus time (entry 2, Table 2).

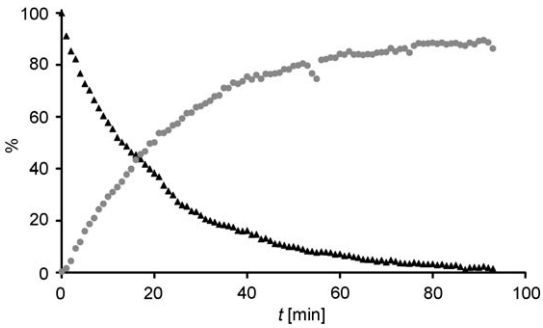

Figure 3. Conversion of silane **3** (▲) and formation of formoxysilane **4** (●) plotted versus time (entry 2, Table 3).

which differs from the experiment shown in Figure 2 only by the later addition of CO_2. The results are given in Table 3.

First, in all experiments employing Method B, silane conversion starts immediately after pressurization of the reactor with CO_2 as shown in Figure 3. The relative order of activity of the precatalysts used is similar to that found in using Method A, which indicates that effects of the oxidation state and of the halide ligand discussed above, apply under both experimental conditions.

Second, there is a tremendous acceleration of silane conversion over the reaction time, which is between a factor of 6.8 (entries 2, Tables 2 and 3) and a factor of 2 (entries 6, Tables 2 and 3), compared with experiments with CO_2 present before the reaction mixture is heated. Due to this acceleration, time resolution reaches the limit of exact determination in the case of the most active catalysis conditions:

Table 3. Hydrosilylation of CO_2 by using Method B (CO_2 added at 358 K).[a]

Entry	Precatalyst[b]	TOF $[h^{-1}]$[c]	Conversion [%][d]	Yield [%][d]	Selectivity [%][d]
1	**5**	3700	92	86	94
2	**6**	1300	99	96	99
3	**7**	980	99	82	83
4	**8**	430	83	79	95
5	**9**	560	95	95	>99
6	**10**	80	>99	77	77
7	**5**[e]	3000	97	91	93
8	**7**[e]	3400	>99	96	97

[a] Conditions (see Experimental Section): 20 mL MeCN, 20 mmol Me_2PhSiH (**3**), $T = 358$ K. [b] 40 μmol. [c] [mol silane **6**]/[mol Ru][t]; based on yields given in the table and calculated from the period when product formation was measured. [d] Values are based on ^1H NMR analysis of the product solution. [e] 2 mmol $Me_2PhSiCl$ added.

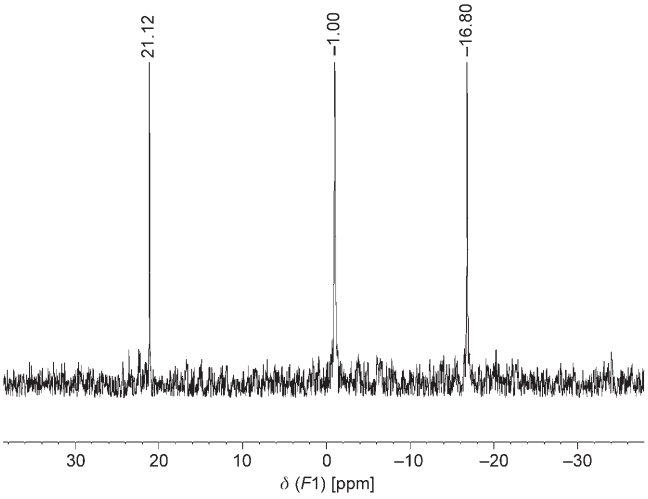

Figure 4. $^{29}Si\{^1H\}$ NMR during the reduction of complex **5** to complex **7** by Me_2PhSiH in MeCN.

Under the prevailing experimental conditions conversion is complete within 6 min at most, which does not allow for sufficient time resolution of the IR analysis.[1]

For entry 1 (Table 3), for instance, the TOF is determined at approximately 3700 [product][Ru]$^{-1}$ h^{-1}, which also underlines the general effectiveness of this synthesis.

Third, pre-activation depends only on the presence of silane: When silane is added after the reaction temperature has been reached, while all other components were added before, no acceleration of conversion is observed, which confirms the assumptions made above.

The effect of the higher activity of Ru^{III} precatalysts is explained by the presence of Me_2PhSiX as an activator, formed by the reduction as shown in Scheme 5.

In a stoichiometric experiment the formation of $Me_2PhSiCl$ as a result of the reduction of complex **5** to complex **7** was proved experimentally by ^1H and ^{29}Si NMR spectroscopy. Already at a reduced temperature (283 K), gas evolution was observed.

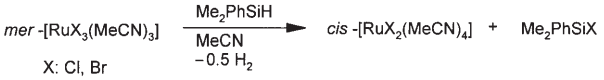

Scheme 5. Reduction of Ru^{III} to Ru^{II} in the presence of silane.

^{29}Si NMR analysis of the reaction solution, in accordance with Scheme 5, at 333 K (to obtain concentrations sufficient for NMR analysis) was performed, which should be related to the catalysis experiments before any CO_2 is added. The spectrum shows three signals at δ −16.8, −1.0 and +21.1 ppm (Figure 4). The resonances at δ −16.8 and +21.1 ppm were identified by comparison with reference samples as silane **3** (−17.2 ppm at 300 K) and $Me_2PhSiCl$ (+21.3 ppm at 300 K), respectively.

Consequently, when starting from Ru^{II}, Me_2PhSiX is not formed and, therefore, also is not present in CO_2 hydrosilylation. To prove whether Me_2PhSiX improves catalytic activity, two additional experiments were performed (entries 7 and 8, Table 3). Together with the Ru^{II} and the Ru^{III} chloride complexes, **5** and **7**, respectively, $Me_2PhSiCl$ was added separately to the reaction mixture. Conversion in the presence of $Me_2PhSiCl$ is accelerated in the case of Ru^{II}, from TOF 1300 to 3400 h^{-1} (entries 2 and 8, Table 3). Otherwise, no significant difference in the reaction rate is found with Ru^{III}, with TOF 3700 and 3000 h^{-1} (entries 1 and 7, Table 3) because $Me_2PhSiCl$ has been already formed by reduction to Ru^{II}, and additional $Me_2PhSiCl$ does not effect catalytic activity. The role of chlorosilanes in the reaction mechanism will be discussed in Section on Catalytic Cycles.

The resonance at δ −1.0 ppm (Figure 4) belongs to an unidentified silicon containing compound. An explanation is that, in the absence of CO_2, the C−N bond of the MeCN solvent is hydrosilylated.[25] One possible product would be Me−CH=N($SiMe_2Ph$). Yet, we were unable to isolate this imine or a related organosilicon product from the reaction with MeCN. On the other hand, it is known that N-silylated imines are particularly unstable as a result of imine–enamine tautomerism[26] or oligomerization. Evidence of this tautomerism was given by in situ IR investigation with prolonged pre-activation (Figure 5).

The initial absorbance at 1676 cm^{-1} probably belongs to Me−CH=N($SiMe_2Ph$) and, while its intensity is decreasing, the absorption at 1612 cm^{-1} is reaching its maximum, which is assigned to the corresponding H_2C=CH−NH($SiMe_2Ph$) enamine. To clarify our assumption, in a preliminary experiment, we performed hydrosilylation of *t*BuCN with Me_2PhSiH catalyzed by complex **5**.[27] *t*Bu−CH=N($SiMe_2Ph$), which cannot undergo enamine formation and which is assumed to be relatively stable to oligomerization, is formed with approx. 70% yield.[2]

[1] The reaction rate is very sensitive to the reaction conditions, particularly to the heating period before CO_2 dosing, which can result in limited experimental reproducibility.

[2] From the analytical data present, no assignment to *Z*,*E* isomers of alkylidene-dimethylphenylsilanyl-amine (primary product) as well as of dimethylphenylsilanyl-vinyl-amines (secondary product from tautomerism) is possible. NMR data suggest imines to be present in one isomer only.

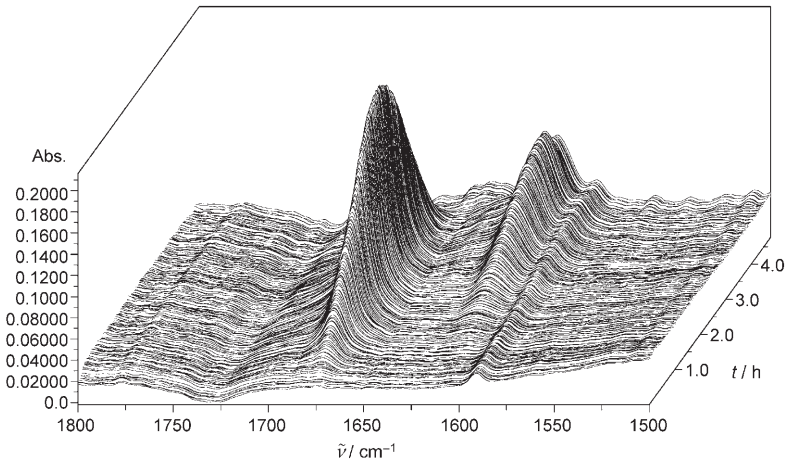

Figure 5. Plot of IR spectra (1500 to 1800 cm^{-1}) versus time for the presumed MeCN hydrosilylation.

Its ν_{CN} absorption of 1688 cm^{-1} is close to the intermediate absorption (1676 cm^{-1}) during the pre-activation in MeCN, as discussed above. Furthermore, the ^{29}Si NMR shift of *t*Bu–CH=N(SiMe$_2$Ph) (−3.1 ppm) is close to the value of −1.0 ppm detected for the presumed MeCN hydrosilylation product (Figure 4), as should be the case for a similar shielding of the ^{29}Si nucleus, which supports the underlying hypothesis.

DFT calculations on potential catalytic pathways

The observations made in the catalysis experiments prompted us to perform quantum chemical calculations on the potential reaction mechanism of CO_2 hydrosilylation. The first assumption was that the oxidation state of the active intermediate before substrate binding is Ru^{II}: Oxidative addition/reductive elimination steps between Ru^{II}/Ru^{IV} are believed to be much more probable under reducing conditions in the presence of silanes, than with the Ru^{III}/Ru^{V} couple. The second assumption was that dissociation of MeCN ligands from the Ru^{II} complexes provides active sites for substrate binding.

Full catalytic cycles were calculated from neutral resting state complexes of composition $[Ru^{II}Cl_2(MeCN)_4]$ and $[Ru^{II}Cl(MeCN)_5]^+$ monocationic species; Me_3SiH was used as a model silane, which minimized the number of conformers to be taken into account. Also for the corresponding bromide compounds $[Ru^{II}Br_2(MeCN)_4]$ and $[Ru^{II}Br(MeCN)_5]^+$, the differences in energy between the resting state and crucial transition states were calculated to explain the halide effect discussed on the previous page. Furthermore, pathways leading to alternative reaction products were considered and will be discussed below.

Comparison of experimental and calculated structures of *cis*-$[Ru^{II}Cl_2(MeCN)_4]$ (7): To make sure that the DFT methods chosen yield reliable structural predictions, we first considered the neutral complex **7**.

Table 4 shows a comparison of experimental and computed structural parameters. As can be seen, experiment (where significant) and theory are in good agreement; a certain overestimation of strong covalent bond lengths (as for the C≡N bond) is typical of this computational method.

For general accuracy of the energetics in organometallic reactions, benchmark calculations have shown the BP86 level of theory to yield satisfactory results.[28] All higher correlated quantum chemical methods would be restricted to the treatment of very simplified model systems anyway.

Table 4. Comparison of experimental and calculated (BP86/SV(P)) structural parameters (bond lengths in Å and angles in °) of complex **7**.

Structural parameter	Experiment	BP86/SV(P)
Ru–N(3/3a)	2.011	1.989
R–N(1/2)	2.092/1.972	1.982
Ru–Cl(1/1a)	2.405	2.405
N(3)–C(5)	1.135	1.173
N(3)-Ru-N(3a)	93.2	95.0
N(3)-Ru-Cl(1)	87.8	86.8
Cl(1)-Ru-Cl(1a)	91.1	91.4

The catalytic cycles: For most stages of the catalytic cycles, several isomers are generally possible, such as *cis*-/*trans* or *fac*-/*mer* structures. Structural diversity is often further increased by the presence of more than two different ligands and/or various rotamers of fragments, such as the orientation of the Me_3Si group with respect to neighboring ligands. As a consequence of this, the lowest energy isomers of intermediates along the catalytic cycle often do not "fit together", that is, there are no (low energy) pathways connecting them.

The catalytic cycle of neutral catalyst complexes, discussed in the following, therefore was constructed under the constraint to contain the most stable transition states. This approach is justified by the Curtin–Hammett principle: Catalysis will mainly proceed via pathways with minimal activation barriers. Furthermore, for both neutral and monocationic intermediate species, energies of the most stable isomers are given to check if these complexes are thermodynamic sinks, which act as second resting states and thus cutting back catalysis.

A first investigation was performed on potential isomerization mechanisms. This was done for the neutral catalyst resting state $[Ru^{II}Cl_2(MeCN)_4]$ and the corresponding coordinatively unsaturated $[Ru^{II}Cl_2(MeCN)_3]$ species, results are given in Scheme 6. Here and throughout the following, L represents MeCN.

MeCN ligands are bound to the Ru centers with energies of about 100 kJ mol^{-1}. As expected, ligand dissociation does not involve any additional activation barriers, that is, MeCN coordination to empty octahedral sites is spontaneous.

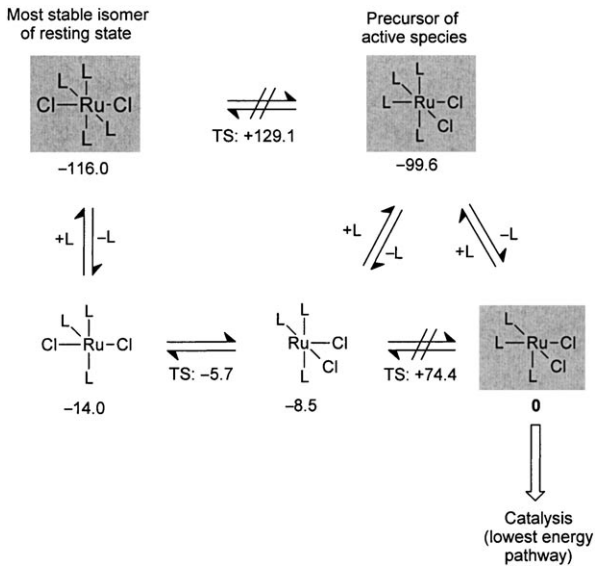

Scheme 6. Calculated relative energies (BP86/TZVP||BP86/SV(P)) in kJ mol^{-1} of intermediates and transition states of neutral catalyst resting state and active species isomers [$Ru^{II}Cl_2(MeCN)_{3/4}$].

Octahedral complexes exhibit high barriers of isomerization, as is the case for the rather hypothetic *cis–trans* conversion of [$Ru^{II}Cl_2(MeCN)_4$], which involves a trigonal prismatic transition state; due to its high relative energy such processes are very unlikely as compared to ligand dissociation.

In the coordinatively unsaturated species [$Ru^{II}Cl_2(MeCN)_3$], the free coordination site allows for much easier isomerization via ligand migration. Cl^- will change places particularly fast, as in the transition state it donates electron density to both old and new coordination site via two of its free electron pairs. Moving MeCN ligands to places between two octahedral coordination sites is not that easy; the thermodynamic equilibration of isomers with different MeCN arrangements will therefore proceed rather as a sequence of ligand association/dissociation.

In summary, Scheme 6 illustrates that an equilibration between isomers is to be expected in general, but equilibration often will involve a number of reactions. This also means that within our idealized model there should be no intrinsic differences in activity between *cis*- and *trans*-Ru^{II} precatalysts.

The most probable[3] catalytic cycle for CO_2 hydrosilylation, according to the DFT calculations described below, is summarized in Scheme 7.[4]

[3] For the sake of simplicity, temporary ligand exchange reactions of the only weakly donating Me_3SiCl, which could give rise to some intermediates lower in energy, have been omitted in this section and will be discussed in the Section on ligand properties of chlorosilanes.

[4] From **E** to **F** a relocation of the chloride ligand has to take place. As complexes with empty coordination sites and chloride *trans* to a hydride ligand are not stable, **F** is formed upon a "displacing entry" of CO_2; the transition state of this process exhibits a relative energy of +21.2 kJ mol^{-1} and thus an activation barrier of almost 50 kJ mol^{-1}, which is not critical, however, if compared to the subsequent rate limiting reaction step.

Energies and Gibbs free energies of stationary points on the potential energy surfaces for both pathways starting from the neutral and the cationic resting states are listed in Table 5; in addition, Figure 6 provides an energetic representation (*E* and *G*) for the reaction profile starting from neutral resting state. At a first glance, the overall activation barrier of the catalytic cycle (about 150 kJ mol^{-1}, starting from the active species) seems prohibitive for a smooth reaction at about 100 °C. However, CO_2 has been treated as an ideal gas in the calculations, which is surely not the case at the reaction conditions applied. The whole *G* profile therefore has to be shifted towards lower values from species **F** on by a certain "real gas" free energy offset, which is difficult to quantify and therefore has been omitted while considering the following. It may be also rationalized from the fact, that experimentally product formation takes place quantitatively, in spite of the overall slightly positive Gibbs free reaction energy.

As mentioned before, not only for transition states, but also in the case of intermediates the potential energy surfaces were scanned to identify the most stable isomers of each complex **A**–**I**. For the neutral complexes a comparison of the isomers used in the catalytic cycle and the lowest energy species is given in Table 6.

General trends in the Ru^{II} complexes with two halide ligands, discussed in the following, are:

1) If both chlorine atoms are present as anions, one observes a higher stability of structures with a *trans*-Cl^- arrangement.
2) This is reversed when one of the anionic ligands is H^-; here, an increased *trans*-repulsion favors the weakest coordinated ligand being in this *trans*-position to the hydride.
3) A number of coordination modes of the CO_2 substrate or the formoxysilane product other than in the catalytic cycle can give rise to isomers of different stability.

Through such effects, there are many cases of intermediates, where the lowest energy isomer is favored by about 50 kJ mol^{-1} with respect to the structure required in the Curtin–Hammett catalytic cycle. However, none of these minimal energy complexes is more stable than the "best" structure of **A**, as required for a smooth catalysis.

Although the structural diversity is less complex for the cationic catalyst resting state [$Ru(MeCN)_5Cl]^+$, there are also a number of isomers need to be taken into account; the most stable structures are compared in Table 7 to the corresponding lowest energy isomers of the neutral catalyst.

One feature of the cycle starting from the cationic resting state is its even higher energetic spread; the energy, required to remove donor ligands from positively charged centers is generally higher than in the case of systems carrying no overall charge.

In the following the catalytic cycle will be discussed in further detail:

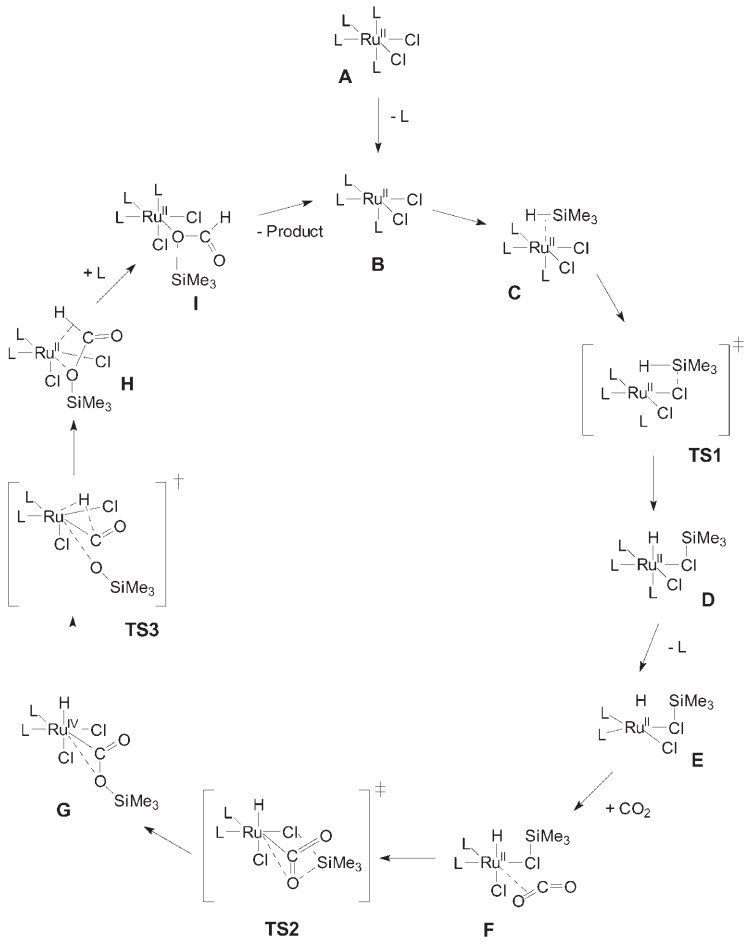

Scheme 7. Calculated mechanism of the hydrosilylation of CO_2 involving a neutral complex of formula $[Ru^{II}Cl_2(MeCN)_4]$ (**A** ≡ **7**) as catalyst resting state.

Catalyst activation

As mentioned before, in analogy to the hydrosilylation of olefins, hydrosilylation of CO_2 can be expected to proceed via a Chalk–Harrod (a) or a modified Chalk–Harrod mechanism (b) as outlined in Scheme 8. In any case at least one MeCN must dissociate first, from the 18 valence-electron catalyst resting states **A**, $[Ru^{II}Cl_2(MeCN)_4]$ and $[Ru^{II}Cl(MeCN)_5]^+$, to enable substrate coordination. As is to be expected, such ligand removal is endothermic (about 100 kJ mol^{-1} for the neutral, and even more for the pathway starting from cationic resting state), but is definitely not that endergonic due to a positive reaction entropy: *G* values, calculated as outlined above are reduced because of the positive $T\Delta S$ term by about 50 kJ mol^{-1} for both neutral and cationic cases.[5]

The neutral and cationic 16-electron Ru^{II} species, **B**, were chosen as reference points for intermediates and transition states in each catalytic cycle, for both *E* and *G*.

Both substrates could now be coordinated to the metal center. However, CO_2 ligands exhibit low binding energies (in both η^1- and η^2-coordination) if attached to Ru^{II} centers, with the consequence that substitution of MeCN by CO_2 is endothermic

Table 5. Calculated (BP86/TZVP||BP86/SV(P)) energies and Gibbs free energies [kJ mol^{-1}] of intermediates and transition states for the hydrosilylation pathway, starting from *cis*-$[Ru(MeCN)_4Cl_2]$ (**A** ≡ **7**), see Scheme 7 and Figure 6.

Complex/Intermediate	rel. *E*	rel. *G* (358 K, 30 bar)
A	−99.6	−52.9
B	0	0
C	−61.9	−7.1
TS1	−17.4	+35.7
D	−64.2	−9.9
E	−27.6	−19.2
F	+5.9	+74.5
TS2	+81.3	+149.7
G	+20.3	+88.8
TS3	+30.6	+94.5
H	+29.2	+98.1
I	−94.2	+28.5
B + product	−57.2	+2.5

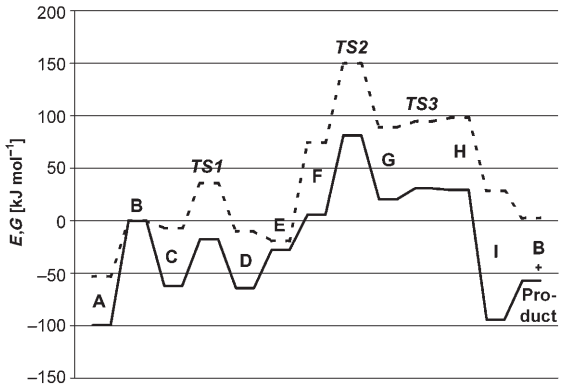

Figure 6. Calculated (BP86/TZVP||BP86/SV(P)) potential energy, *E* profile (——), and free enthalpy, *G* profile (-----), for the catalytic cycle involving neutral complexes.

[5] The degree of endothermicity for opening up the coordination sphere around transition metal centers is also partly due to a basis set superposition error. It should also be noted, that with the hybrid functional B3LYP, MeCN-dissociation energies are about 10 kJ mol^{-1} lower than within BP86.

Table 6. Comparison of calculated (BP86/TZVP||BP86/SV(P)) energies [kJ mol^{-1}] of intermediates involved in the Curtin-Hammet catalytic pathway (Scheme 7 and Figure 6) and actual minimum energy isomers for the hydrosilylation pathway, starting from a catalyst composition [Ru(MeCN)$_4$Cl$_2$]. Transition state energies (entries in gray) are given for comparison as well.

Complex/ Intermediate	Isomer used in catalytic cycle	Minimum energy isomer	Structure of minimum energy isomer
A	−99.6	−116.0	Cl$^-$ *trans*
B	0	−14.0	Cl$^-$ *trans*
C	−61.9	−77.6	Cl$^-$ *trans*
TS1	−17.4	–	–
D	−64.2	−112.2	Me_3SiCl *trans* w. resp. to H$^-$
E	−27.6	–	–
F	+5.9	−34.2	CO_2 η^1 and *trans* w. resp. to H$^-$, L *cis*
TS2	+81.3	–	–
G	+20.3	−0.5	Cl$^-$ *trans*, L *trans*
TS3	+30.6	–	–
H	+29.2	−18.4	Cl$^-$ *trans*, $HCOOSiMe_3$ η^2-coordinated via both O
I	−94.2	−143.6	Cl$^-$ *trans*, $HCOOSiMe_3$ coordinated via C=*O*

Table 7. Calculated (BP86/TZVP||BP86/SV(P)) energies of minimum energy intermediates and transition states for catalytic hydrosilylation.

Complex/ Intermediate	neutral complexes, starting from [Ru(MeCN)$_4$Cl$_2$]	cationic complexes, starting from [Ru(MeCN)$_5$Cl]$^+$
A	−116.0	−140.0
B	−14.0	0
C	−77.6	−86.6
TS1	−17.4	−42.3
D	−112.2	−143.2
E	−27.6	−34.1
F	−34.2	−40.9
TS2	+81.3	+111.3
G	−0.5	+13.7
TS3	+30.6	+37.8
H	−18.4	−22.1
I	−143.6	−139.7

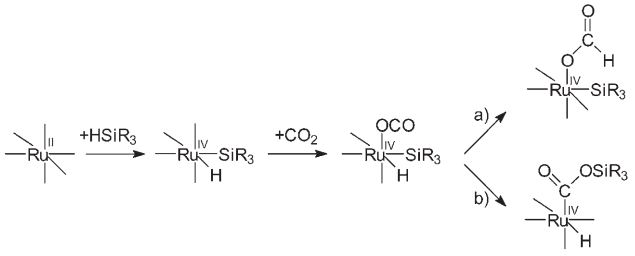

Scheme 8. Chalk–Harrod (a) and modified Chalk–Harrod (b) mechanisms of CO_2 hydrosilylation.

and even more endergonic, as CO_2 is treated as a gas in the *G* calculation. Therefore, intermediate and transition-state complexes with CO_2 as a pure spectator ligand will play no role in a minimum Gibbs free energy catalytic cycle. We thus continued by first investigating the postulated silane oxidative addition which should occur in both mechanistic scenarios mentioned above.

Oxidative silane addition versus silane metathesis

Although one free coordination site is sufficient to bind the silane by side-on interaction of the Si–H bond to the Ru center (as in **C**), oxidative addition requires dissociation of another MeCN ligand.[6]

In the immediate reaction product, the H and the Me_3Si groups would always be generated *cis* with respect to each other. All geometry optimizations of such tentative oxidative adduct structures, however, resulted in complexes with the Si–H bond more or less restored as a purely side-on coordinating σ_{Si-H} bond, utilizing only one coordination site (and sometimes a RCH_2–H bond interacting agostically with the remaining sixth octahedral corner), see Figure 7. Experimental evidence for such binding mode in other Ru^{II} complexes with similar Si–H bond lengths has been reviewed by Nikonov[29] and Sabo–Etienne et al.[30] The latter authors emphasize the fact that there is a continuous transition between σ-bonded complexes and oxidative adduct—in the case of our Ru complexes, the bonding situation corresponds predominantly to the sigma-bonding state.

As a consequence, these resultant complexes exhibit a fairly open or just weakly saturated coordination site, which makes them rather unstable.

We also optimized the geometry of sixfold-coordinated *trans*-H$^-$/Me_3Si^- complexes, which, however, have either high energies or exhibit strongly distorted structures with rather short distances between the Me_3Si moiety and other ligands, for example, Cl$^-$. Within B3LYP, all oxidative *trans*-adducts are destabilized even more strongly by another 40 kJ mol^{-1}.

These findings clearly indicate that also organosilanes similar to Me_3SiH containing Si–H bonds are unable to act as oxidants when added to Ru^{II} (at least in the presence of the rather poorly σ-basic MeCN environment). However, for CO_2 hydrosilylation to proceed in the manner observed, some kind of Si–H activation step cannot be avoided; as oxidative addition is not possible, this activation could occur by metathesis of the Si–H bond. Two such processes were considered here:

Direct Si–H dissociation onto the Ru-CO_2 moiety (Scheme 9): This reaction is possible in principle, but exhibits a rather high activation energy (pathway starting from neutral resting state: +137.2 kJ mol^{-1}, pathway starting from neutral resting state: +157.2 kJ mol^{-1} with respect to the activated catalyst; due the consumption of CO_2 from the gas

[6] Ru^{IV} structures with seven ligands were tried in a large number of calculations, but either rearranged to sixfold coordinate silane or chlorosilane complexes, lost one acetonitrile or resulted in strongly destabilized species (more than 100 kJ mol^{-1} less stable than Si–H side on reference complexes for the neutral case).

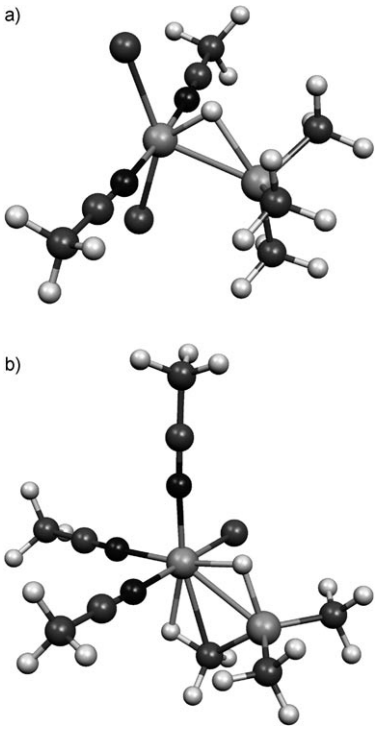

Figure 7. Calculated structures of the most stable isomers of [Ru(MeCN)$_2$Cl$_2$-*cis*-(η^2-Me$_3$Si-H)] (top, with $d_{Si-H}=2.017$ Å) and [Ru(MeCN)$_3$Cl-*cis*-(η^2-Me$_3$Si-H)]$^+$ (bottom) with $d_{Si-H}=2.017$ Å (BP86/SV(P)). Geometry optimization started in each case from octahedral complexes [Ru(MeCN)$_2$-*cis*-Cl$_2$-*cis*-(Me$_3$Si)(H)] and [Ru-*fac*-(MeCN)$_3$Cl-*cis*-(Me$_3$Si)(H)]$^+$, respectively.

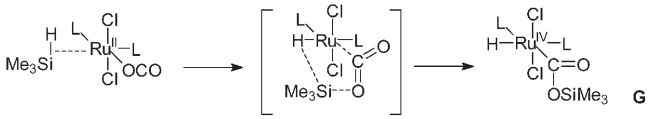

Scheme 9.

phase, Gibbs free activation energies are additionally increased by some 60 kJ mol^{-1}). We therefore looked for an alternative pathway also able to account for formoxysilane formation.

Silyl transfer to chloride ligands: As mentioned above, the Si–H bond can also dissociate by (here again) forming a Ru–H bond and a chlorosilane ligand, which results in complex **D** (Scheme 10).

This metathesis is much more favorable, the energy of transition state **TS1** being even lower than that of the catalytically active species (e.g. neutral case: -3.3 kJ mol^{-1}), which is a consequence of the saturated coordination sphere around Ru^{II} in the reactant, product and transition state. The activation barrier with respect to the neutral side-on silane complex precursor is around 45 kJ mol^{-1}.

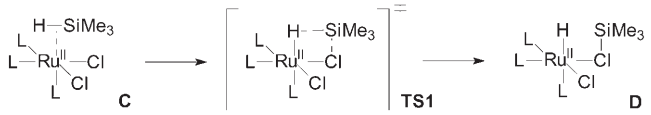

Scheme 10.

We also checked if metathesis reaction steps could occur with a silyl transfer to the metal center, but were able to characterize such processes as insignificant.

Rate limiting silyl transfer to CO_2

The highest point on a minimum energy (as well as Gibbs free energy) pathway for CO_2 hydrosilylation was found to be the subsequent silyl transfer from the R_3SiCl ligand to the oxygen atom of a η^2-bound CO_2 (**TS2**) (Scheme 11).[7]

The resulting complex (**G**) is identical to that of process a), direct Si–H dissociation onto a CO_2 complex (see section above); the pathway leading to it, however, is energetically much more preferable (neutral catalyst: $+81.3$ kJ mol^{-1} higher than the active complex reference on a potential energy surface).

The detour via a Me_3SiCl ligand leads to a lower energy pathway because:

1) in all precursors of the rate limiting transition state, the energy of silane substrate (i.e., its reactivity) is "conserved"; the higher Si–Cl bond energy is compensated by the reduced ligand binding energy of the chlorosilane;
2) the polarity of chlorosilane (much stronger δ^+ at Si as compared to Me_3SiH) favors a silyl transfer to $O=C=O$, that is, the oxophilicity of Si is increased in the intermediate Me_3SiCl complex **F**.

In **G**, the metal center formally is Ru^{IV}. However, with -C(=O)OSiR$_3$, there is a more electronegative ligand attached to it than would be the case with -SiR$_3$ in a hypothetical silane oxidative adduct.

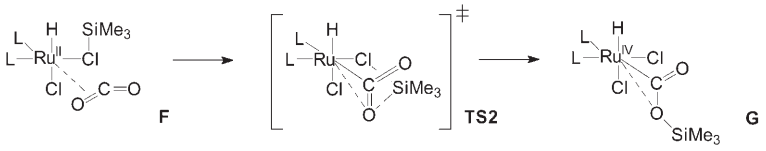

Scheme 11.

[7] In principle, similar transition states involving several chlorosilane molecules and thus larger rings as reaction centers are possible as well (though disfavored entropically). However, a tentative transition state (involving two Me_3SiCl) with a seven-membered ring turned out to be about 50 kJ mol^{-1} higher in energy than **TS2**, indicating that only species with five-membered rings and one chlorosilane are in fact relevant.

Reductive elimination/Product release

From the formal Ru^{IV} complexes, **G**, a reductive elimination step **TS3** yields the formoxysilane product and regenerates a Ru^{II} species, **H**. As this reaction step is connected with the formation of an open coordination site at the metal center, it is slightly endothermic. Compared to the silyl transfer, **TS2**, the activation barrier for the sequence **G** → **TS3** → **H** is rather small.

The subsequent addition of another MeCN ligand, leading to **I**, is strongly favored energetically (by more than 100 kJ mol^{-1}), which makes product formation irreversible. Subsequent product release regenerates the active catalyst, **B**; this, of course, is an endothermic step (pathway starting from neutral resting state: +37.0 kJ mol^{-1}), but not as endothermic as catalyst activation starting from **A**, and even thermodynamically preferred on a Gibbs free energy surface, taking entropy effects into account. This means that catalyst activity will not suffer from product inhibition, which is still the case, if one considers the optimal coordination mode of the formoxysilane as outlined in Table 8.

Table 8. Selected calculated (BP86/SV(P)) atomic distances and bond angles of complexes involved in the catalytic cycle starting from neutral resting state (Scheme 7 and Figure 6).

Complex/Intermediate	Structural feature	Bond length [Å] or angle [°]
C	d(Ru–H)	1.757
	d(Ru–Si)	3.036
	d(Si–H)	1.580
TS1	d(Ru–H)	1.636
	d(Ru–$Cl_{reacting}$)	2.458
	d(Si–H)	2.149
	d(Si–Cl)	2.353
D	d(Ru–H)	1.608
	d(Ru–$ClSiMe_3$)	2.554
	d(Si–Cl)	2.178
	(Ru-Cl-Si)	113.5
F	d(Ru–O)	2.155
	d(Ru–C)	2.137
	(O-C-O)	143.1
TS2	d(Ru–$Cl_{reacting}$)	2.399
	d(Si–Cl)	2.680
	d(Si–O)	2.054
	d($O_{reacting}$–C)	1.373
	d(Ru–CO_2)	2.013
	d(Ru–O)	2.149
	d(H–CO_2)	2.011
G	d(Ru–H)	1.606
	d(Ru–C)	1.991
	d(C–$OSiMe_3$)	1.386
	d(Ru–O)	2.200
TS3	d(Ru–H)	1.662
	d(C–H)	1.497
	d(Ru–O)	2.289
I	d(Ru–O)	2.255

Overall reaction energy/Gibbs free energy

Hydrosilylation of CO_2 by Me_3SiH is predicted to be an exothermic reaction ($\Delta E = -57.2$ kJ mol^{-1}). Its Gibbs free energy under idealized reaction conditions of 85 °C and a CO_2 pressures of 30 bar is almost zero ($\Delta G = +2.5$ kJ mol^{-1}) or just slightly exergonic within B3LYP ($\Delta G = -4.1$ kJ mol^{-1}). In a more realistic view, however, CO_2 does not behave as an ideal gas anymore, as mentioned before, which means that the statistical thermodynamic formulae are bound to overestimate the entropy loss resulting from CO_2 fixation. Therefore, also from a quantum chemical point of view, complete conversion of silane and CO_2 to formoxysilanes is possible.

Structural features of intermediates and transition states: Structures of intermediate and transition state complexes occurring in the reaction pathway starting from neutral resting state of Scheme 7 are shown in Figure 8.

In all complexes, there are chloride and MeCN ligands around Ru. Typical bond lengths for the Ru^{II}–Cl and Ru^{II}–N bonds are 2.40–2.45 and 1.9–2.0 Å, respectively, as found already for the crystallographically characterized resting state isomer in the Section on Comparison of the Structure of *cis*-[$Ru^{II}Cl_2(MeCN)_4$]. Especially the length of the Ru–N bond, however, is strongly dependent on the ligand *trans* to it (e.g. in the product of the silyl transfer from H^- to Cl^-, **D**, $d_{Ru-N} = 2.141$ Å for the MeCN *trans* to the hydride). Characteristic bond lengths and angles are presented in Table 8.

In **C**, Me_3SiH as the first substrate enters the catalytic cycle. The fact, that the Si–H bond in **C** acts as a side-on ligand is reflected by an increased Si–H bond length from 1.515 Å in the free silane to 1.580 Å. With 1.757 Å, the Ru–H distance is still rather long here, if compared to the hydride complexes like **D** or **G**, where the Ru–H distance is shorter by about 0.15 Å.

After the silyl migration of **TS2**, which involves a hypervalent Si center, the catalytic cycle contains several complexes with a Me_3SiCl ligand. This neutral two electron donor is not bound as strongly to the Ru center as Cl^-. In complexes like **D** one therefore observes an increase of the corresponding Ru–Cl distances by about 0.1 Å. Upon coordination to the metal center, the Si–Cl distance of free Me_3SiCl (2.113 Å) on the other hand is also increased by more than 0.05 Å.

Being a double-bonded system with free electron pairs at O, CO_2 can bind η^1 and η^2 to a transition-metal center.[31] It is found, that both coordination modes are rather similar in energy (e.g. an isomer of **F** in which just the coordination of CO_2 has been changed towards η^1, $d_{Ru-O} = 2.202$ Å, is only 3.1 kJ mol^{-1} less stable than **F** itself). As already mentioned, the CO_2 substrate exhibits rather poor ligand properties, the weakness of its (non-reactive) interactions with Ru^{II} can be estimated from the *trans*-effect in the most stable isomer of **F**, where the repulsion of the *trans*-H^- ligand leads to a Ru–O bond length of 2.603 Å.

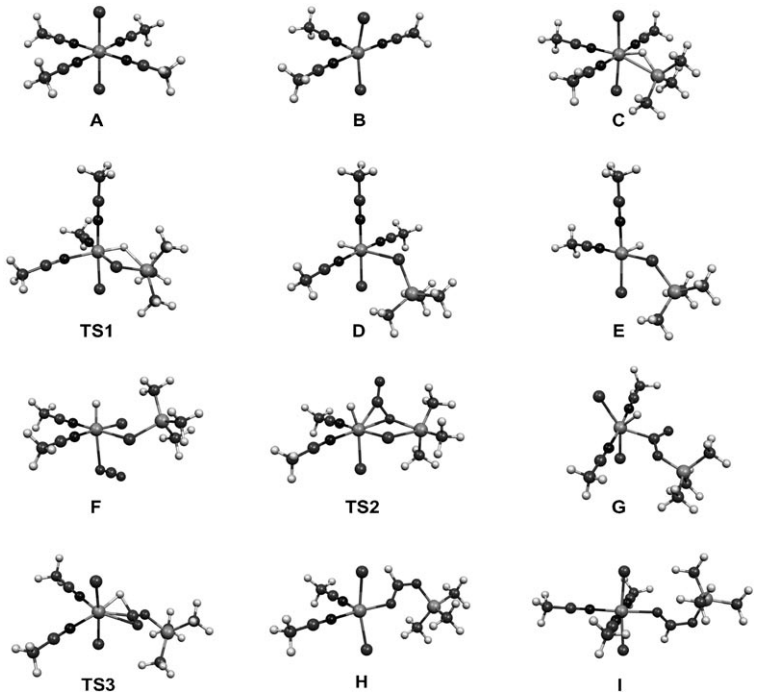

Figure 8. Calculated structures (BP86/SV(P)) of intermediate and transition state complexes for a catalytic pathway starting from neutral resting state.

In the rate limiting silyl transfer step **TS2**, however, a *cis*-arrangement of a η^2-CO_2 and H^- is preferred; the strongly polar Ru–H bond even seems to be a prerequisite for fixing CO_2 by a local dipole-dipole interaction between $Ru(\delta^+)$ and $O(\delta^-)$ as well as $H(\delta^-)$ and $O_2C(\delta^+)$.[8]

The quasi η^2-C=O coordination in **TS2** is maintained in migration product **G**. Also for the reductive elimination step, **TS3**, a quasi η^2-formate group turned out to be most stable. **TS3** is altogether rather product like; in the resulting **H**, the free coordination site is stabilized by the formoxysilane product acting as a four electron-donating ligand at both coordination sites available: However, unlike in the outcome of **TS3**, where the elimination product is attached to the metal via Me_3Si-*O*-CHO and an agostic interaction with the formyl C–H bond, much more stable coordination of the product can be achieved if it is effected by both oxygen atoms. If only one donor is needed, it turns out that the carbonyl O of the formoxysilane binds most strongly to Ru^{II}, which is another reason why catalytic cycle structure **I** is not the most stable isomer.

Silyl migration to/from bromide ligands: With the halide ligand directly involved in the catalytic cycle via intermediate halosilane formation, it is not surprising that various halide ligands exhibit different catalyst activities, as was discussed in the Section on in situ monitoring of CO_2 hydrosilylation above. The catalytic turnover numbers observed decrease in the order of $Cl^- > Br^-$ for all complexes experimentally investigated. Table 9 shows for the bromide case how replacement of chloride ligands by its heavier congeners raises the relative energies (with respect to the catalyst resting state, **A**, and active species, **B**) of both **TS1** and **TS2** by at least 10 kJ mol^{-1}.

Destabilization of the transition states in the bromide case is a consequence of the generally lower Si–Br bond energies compared with Si–Cl. The resultant higher energetic spread of the energy profile, that is, difference between the resting state and the rate-limiting step means lower catalytic activity: The experimental findings are reproduced correctly.

[8] It was found impossible to locate any **TS2**-complexes without this structural motif.

Table 9. Calculated potential energies E [kJ mol^{-1}] (BP86/TZVP||BP86/SVP(P)) of most stable isomers of the resting state **A**, active species **B** as well as transition states, **TS1** and **TS2**, for neutral catalysts with Cl^- and Br^- as halide ligands.[a]

	X = Cl$^-$[a]	X = Br$^-$
A	−102.0	−103.9
B	0	0
TS1	−3.3	+10.6
TS2	+95.3	+106.6

[a] Note: Other reference than in the neutral catalytic cycle energy of the most stable, that is, *trans*-isomer of **B** is set to zero.

Competing reactions

MeCN hydrosilylation: The chlorosilano hydrido complex **D** should be a silyl donor to any substrate with sufficiently polarized C=X or C≡X unit. With the MeCN solvent, one such potential substrate is present under reaction conditions. The reactivity of nitriles in preliminary experiments has been discussed above. This prompted us to investigate theoretically, with the Ru catalysts used here, whether the carbonyl group of CO_2 really is more reactive than the cyano group of nitriles.

In analogy to **TS2**, there should be silyl transfer from a chlorosilane ligand to an η^2-coordinated MeCN. Such a coordination mode was found to be possible in principle, though some 60 kJ mol^{-1} higher in energy than the usual η^1-complexes (which means a η^2-MeCN–Ru^{II} bond energy of about 40 kJ mol^{-1}). For the most stable silyl transfer transition state, we calculated for a pathway starting from neutral resting state (Scheme 12) a relative E of +24.1 kJ mol^{-1} and G

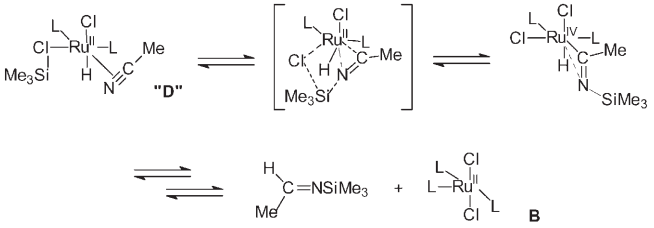

Scheme 12. MeCN hydrosilylation pathway.

of $+58.4\,kJ\,mol^{-1}$ (with respect to the usual reference **B** from the catalytic cycle starting from neutral resting state). Silyl transfer to MeCN therefore should proceed much faster than transfer to CO_2. Thus, subsequent reductive elimination steps were treated computationally as well and found to proceed even more easily.

Thermodynamics answer the question why, in spite of these findings, CO_2 is hydrosilylated in MeCN solution: The formation of silyl imines (at least primarily) results in *cis*-silyl imines, which are rather high in energy and thus themselves can act (indirectly via the fast equilibration with chlorosilane species) as silylating agents.

As this prompted us to perform a number of other investigations on the synthetic potential of nitrile hydrosilylation with Ru catalyst systems, more detailed results will be presented in near future.

Disiloxane formation: The experiments indicate the formation of disiloxanes, which means a reduction of CO_2 by the silane without coupling of the two substrates.

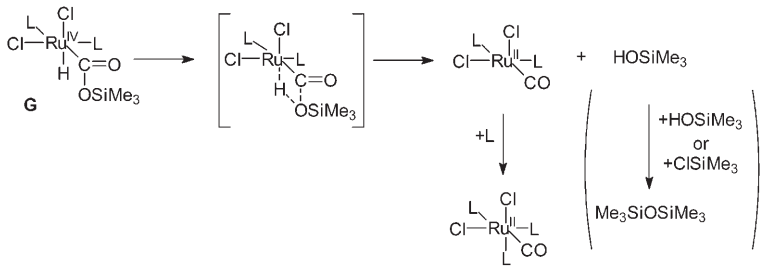

Scheme 13. Disiloxane formation pathway.

One possibility of such a reaction could be initiated by reductive elimination of a silanol molecule from a suitably oriented isomer of **G** (Scheme 13). Reductive elimination of R_3SiOH as a potential side reaction of the calculated mechanism consequently is accompanied by the formation of $L_nRu(CO)$. Catalytic activity of carbonyl complexes formed in this way, was not considered in calculations but, analogous intermediates as discussed above with one or more CO ligands instead of MeCN could be imagined.

The overall reaction to the silanol and the neutral carbonyl complex of the composition $[Ru(MeCN)_3Cl_2(CO)]$ is strongly exothermic (pathway starting from neutral resting state: $E=-185.9\,kJ\,mol^{-1}$ with respect to reference **B** of the catalytic cycle, silane and CO_2) and thus favored much more strongly from a thermodynamic point of view than formoxysilane formation; however, the transition state of the required alternative reductive silanol elimination is of rather high energy (pathway starting from neutral resting state: $E=+90.5\,kJ\,mol^{-1}$ with respect to **B**): according to these figures silanol formation (and subsequent condensation with either another silanol or a chlorosilane intermediate to disiloxanes) is disfavored kinetically, as is to be expected from the experiments.

Although no carbonyl complexes have been isolated after catalysis yet, there were experimental hints to their formation from a previous investigation:[32] Using complex **11** in CO_2 hydrosilylation, the solid residue remaining after separation of the organic compounds showed significant absorptions (1971, $2283\,cm^{-1}$) which relate to ruthenium bound carbonyl and nitrile ligands,[33] as well as a broad resonance in solid state ^{13}C NMR at 213 ppm, typical of carbonyl complexes.[9]

Second, when $[RuCl_2(PPh_3)_3]$ is used as precatalyst in a MeCN solution, crystalline $[Ru(CO)_3(PPh_3)_2]$ is isolated reproducibly after CO_2 hydrosilylation.

Ligand properties of chlorosilanes: The calculations clearly indicate that halosilane complexes are involved in the catalytic cycle. Compared with Cl^- and MeCN, Me_3SiCl represents a rather weakly bound ligand. Therefore, Me_3SiCl dissociation from **D**, **E** and **F** (and substitution by for example, MeCN) will play a major role under reaction conditions.

To get an idea of typical ligand binding energies of chlorosilanes, we computationally studied the overall energetics for two different Me_3SiCl replacement reactions with MeCN as the competing ligand, which are outlined in Scheme 14: Substitution of the chlorosilane in the most stable isomer of **D** taking place *trans* with respect to the hydride ligand (a), and the MeCN

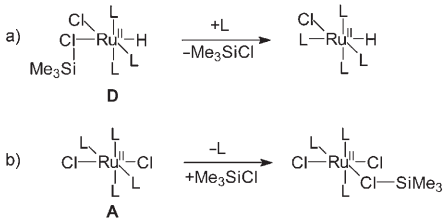

Scheme 14. Ligand substitution steps involving Me_3SiCl.

[9] Also an intensive IR absorption at $2124\,cm^{-1}$ was observed, to be assignable as the ν_{SiH} mode of residual Me_2PhSiH, whereas the related δ_{SiH} absorbance is very weak in intensity, contrasting to pure Me_2PhSiH. Yet, no isolation nor enrichment of Ru complexes from this mixture has been successful.

versus Me_3SiCl exchange in the coordination sphere of the catalyst resting state **A** (reaction b).

In the case of a), any ligand *trans* to H^- is only weakly bound; this means that energetic differentiation between donor ligands is greatly reduced, and the corresponding energy difference is quasi zero ($\Delta E = +4.0\ kJ\,mol^{-1}$, $\Delta G = -4.6\ kJ\,mol^{-1}$). On the other hand, if substitution takes place *trans* to an only moderately strongly bound ligand (like MeCN), as in **b**, the replacement of MeCN by R_3SiCl is endothermic: $\Delta E = +45.6\ kJ\,mol^{-1}$, $\Delta G = +53.2\ kJ\,mol^{-1}$.

This means that (re)coordination of the halosilane to the hydrido complexes (as second resting states) is part of the catalyst activation on the way to the rate limiting silyl transfer step **TS2**. With these findings, the higher catalytic activities observed with additional chlorosilane are no surprise, as the formation of intermediates **D**, **E**, **F** and consequently also **TS2** is more favorable in the presence of an excess of chlorosilane.

Concluding Remarks

Mixed nitrile/halide complexes of ruthenium turn out to be the best choice as catalysts for converting CO_2 to formoxysilanes by hydrosilylation, not only because of their convenient synthesis, but also due to excellent activities. The observed interrelation to the hydrosilylation of the MeCN solvent opens the perspective for further investigations on hydrosilylation of different C–X multiple bonds. The general orders of activity for CO_2 hydrosilylation were found to be $RuCl_mL_n > RuBr_mL_n$ and $Ru^{III} > Ru^{II}$. A Me_3SiH model was used to analyze by DFT methods the most probable pathway of CO_2 hydrosilylation with $[RuX_m(MeCN)_n]^{y+}$ ($y = 0, 1$). The results explain the experimental findings, that is,

- that chloride complexes exhibit higher activities than their analogous bromide derivatives,
- that Ru^{III} precatalysts, due to the initial formation of R_3SiX, are more active than their Ru^{II} analogues (one halide ligand substituted by MeCN), and
- that Ru^{II} (pre)catalysts are more active in the presence of R_3SiCl.

We believe that the calculated key intermediates for the Me_3SiH reaction are similar in energy in the case of Me_2PhSiH, which was used in the catalysis experiments. The most surprising finding from DFT calculations is the silane activation which takes place in a very uncommon fashion by transfer of the Me_3Si unit to a chloride ligand. The presence of R_3SiCl as ligand for silyl transfer to CO_2 in the catalytic cycle is also supported from experiments. To the best of our knowledge, no similar intermediates have been postulated before for a catalytic hydrosilylation cycle. Usually, activation is assumed to take place via oxidative addition leading to $L_nRu(H)(SiR_3)$ or, via a non-classical interaction, resulting in intermediates with side-on coordinating H-SiR_3. Here, we assume the formation of $[L_nRu(ClSiR_3)]$-type intermediates. Although similar stable complexes have not been reported in the literature so far, investigations with related bonding situations are known. Horton et al. reported the synthesis and structure of the chelate complex *rac*-$[C_2H_4(indenyl)_2Zr\{CH(SiMe_2Cl)(SiMe_3)\}][Al_2Cl_{6.5}Me_{0.5}]$ with Si–Cl coordination to an electron-deficient Zr center (Figure 9, complex **I**). The Zr–Cl and Cl–Si bond lengths were determined by X-ray analysis to be 2.57 and 2.27 Å, respectively.[34] Similar interactions, $[L_nM(ClCR_3)]$ and $[L_nM(ClSnR_3)]$, are also known from the literature.[35,36] Reactions of chlorosilanes with activated Pt^{II} complexes were calculated recently, taking into account also $[L_nPt(ClSiR_3)]$ intermediates.[37] Most recently, Nikonov et al. succeeded in the isolation and structural determination of $[Cp^*(iPr_3P)Ru(Cl)(\eta^2\text{-}HSiClMe_2)]$.[38]

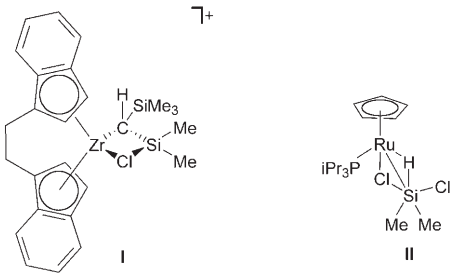

I II

Figure 9. Literature reported complexes with coordinating chlorosilanes.[35,39]

The interactions of the $HSiClMe_2$ ligand in the Ru^{II} complex **II** (Figure 9) formed by the reaction of $[Cp^*(iPr_3P)Ru(Cl)]$ with $HSiClMe_2$ were found to be simultaneously Si–H (1.99 Å), Ru–Si (2.40 Å), Ru–Cl (2.41 Å) and Si–Cl (2.16 Å). This situation is comparable to the calculated neutral transition state (**TS-1**) of Me_3SiH activation in this work (see Section on Structural Features), with Si–H (2.15 Å), Ru–Si (3.11 Å), Ru–Cl (2.46 Å) and Si–Cl (2.35 Å), with the difference that, in **TS-1**, the Ru–Si distance is significantly longer.

Further investigations will also focus on potential reaction pathways via halosilanes in hydrosilylation of other substrates. Particularly, preliminary experiments have given rise to the expectation that C≡N triple bonds in nitriles, which are known to be less reactive in hydrosilylation, can be generally activated by the same type of precatalysts.

Experimental Section

General procedures: All manipulations were carried out under an atmosphere of dry argon. $RuCl_3{\cdot}n\,H_2O$ (**1**) and $RuBr_3{\cdot}n\,H_2O$ (**2**) were purchased from Aldrich, Me_2PhSiH (**3**) from ABCR, PPh_3 from Fluka. All these substances were used without further purification, except for silane **3** which was distilled before use. Solvents were dried and distilled before use according to literature procedures, and stored under argon. Deuterat-

ed solvents were dried over molecular sieves and kept under an inert atmosphere. CO_2 (4.8) was purchased from Messer-Griesheim.

Reactions under CO_2 pressure were performed in a 65 mL stainless steel reactor equipped with a pressure gauge, thermocouple, and magnetic stirrer. $Me_2PhSiOCHO$ (**4**) yields relate to the molar amount of **3**. Byproducts were identified by ^1H and ^{29}Si NMR spectroscopy.

Analyses: The NMR spectra were recorded on a Bruker Avance 250 spectrometer at 298 K. ^1H NMR: 250.130 MHz, internal reference from residual proton signals of the CD_3CN ($\delta = 1.90$) or D_2O ($\delta = 4.85$) solvents, both relative to $SiMe_4$ ($\delta = 0$ ppm); $^{29}Si\{^1H\}$ NMR: 49.694 MHz, internal reference, $SiMe_4$ ($\delta = 0$ ppm). Chemical shifts and coupling constants are given in ppm and Hz, respectively. IR spectra were recorded on a Perkin-Elmer System 2000 FT-IR as a Nujol film (Nujol dried with K/Na alloy), in KBr (dried at 773 K for 12 h) or directly from reaction solutions. Elemental analyses were performed on a CNSO elemental analyzer (Elementar Analysensysteme GmbH).

***mer*-[$RuCl_3(MeCN)_3$] (5) and *mer*-[$RuBr_3(MeCN)_3$] (6)**: $RuX_3 \cdot n H_2O$ (5 mmol) was dissolved in dry MeCN (50 mL) and stirred for 20 h at 353 K. After cooling, the solution was filtered at room temperature and, after removal of volatile components at 10^{-1} mbar, the complexes were dried in a vacuum, yielding 94% orange-red **5** and 83% purple **6**, respectively. When the reaction was performed at a temperature below 353 K, *mer*-[$RuX_3(MeCN)_3$] was isolated as the only product. When the reaction was performed at a higher temperatures, as in the case of **5**, [{Ru^{IV}-*fac*-Cl_3-*cis*-$(MeCN)_2$}$_2$O] was isolated as a by-product. This complex has previously been described by Dehand et al.,[17] but was prepared more easily by refluxing a solution of $RuCl_3 \cdot n H_2O$ (5.11 mmol) and NBu_4Cl hydrate (3.4 mmol) in MeCN (60 mL) for 5 h followed by the addition of Et_2O (60 mL) after cooling to 298 K and crystallization at 277 K.

Elemental analysis calcd (%) for $C_6H_9N_3Cl_3Ru_1$ (**5**, 330.8 g mol^{-1}): C 21.80, H 2.74, N 12.71; found: C 21.86, H 2.98, N 12.76; ^1H NMR (CD_2Cl_2): $\delta = -15.6$ (s, 6H), 47.8 ppm (s, 3H); IR (KBr): $\tilde{\nu} = 2977$ (s), 2920 (vs), 2321 (s), 2294 (vs), 1413 (s), 1367 (m), 1028 (m), 948 (w), 454 cm^{-1} (m).

Elemental analysis calcd (%) for $C_6H_9N_3Br_3Ru_1$ (**6**, 464.1 g mol^{-1}): C 15.53, H 1.96, N 9.06; found: C 16.17, H 1.96, N 8.97; ^1H NMR (CD_2Cl_2): $\delta = -14.9$ (s, 6H), 39.4 ppm (s, 3H); IR (KBr): $\tilde{\nu} = 2970$ (s), 2915 (s), 2327 (m), 2289 (s), 1646 (s), 1419 (s), 1364 (s), 1028 (vs), 946 (s), 452 cm^{-1} (s).

***cis*-[$RuCl_2(MeCN)_4$] (7) and *cis*-[$RuBr_2(MeCN)_4$] (8)**: Silane **3** (8.17 g, 60 mmol) was added slowly to a cold solution of *mer*-[$RuX_3(MeCN)_3$] (3 mmol) in dry MeCN (100 mL). The reaction mixture was kept in an ice bath and stirred for another 5 h while the color changes from deep red to orange in the case of **7**. Crystals of **7** and **8**, respectively, were obtained from the reaction solution after 48 h at 263 K. The product was filtered and washed, first with an excess of diethyl ether, then with pentane, and dried in vacuum. The complexes were recrystallized from MeCN, yielding 80% (**7**, yellow) and 64% (**8**, red), respectively.

Elemental analysis calcd (%) for $C_8H_{12}N_4Cl_2Ru_1$ (**7**, 336.4 g mol^{-1}): C 28.58, H 3.60, N 16.67; found: C 29.51, H 3.80, N 16.29; ^1H NMR (CD_2Cl_2): $\delta = 2.52$ (s, 3H), 2.51 ppm (s, 3H); IR (KBr): $\tilde{\nu} = 2974$ (s), 2915 (s), 2276 (vs), 1650 (m), 1420 (m), 1364 (s), 1035 (vs), 942 cm^{-1} (w).

Elemental analysis calcd (%) for $C_8H_{12}N_4Br_2Ru$ (**8**, 425.3 g mol^{-1}): C 22.60, H 2.85, N 13.18; found: C 22.81, H 2.89, N 13.36; ^1H NMR (CD_2Cl_2): $\delta = 2.54$ (s, br); IR (KBr): $\tilde{\nu} = 2958$ (vs), 2909 (vs), 2277 (vs), 1421 (s), 1035 (s), 946 (s), 799 (w), 669 cm^{-1} (w).

***trans*-[$RuCl_2(MeCN)_4$] (9) and *trans*-[$RuBr_2(MeCN)_4$] (10)**: A solution of *mer*-[$RuX_3(MeCN)_3$] (2.5 mmol) in dry MeCN (100 mL) was cooled to 273 K. Then PPh_3 (40 mmol), dissolved in dry MeCN (150 mL), was added. The reaction mixture was kept at this temperature for another 5 h. Crystals were obtained from the reaction solution after several days at 263 K. The product was filtered and washed, first with an excess of diethyl ether, then with pentane, and dried in a vacuum. The complexes were recrystallized from MeCN, yielding 72% (**9**, orange) and 58% (**10**, orange), respectively.

Elemental analysis calcd (%) for $C_8H_{12}N_4Cl_2Ru_1$ (**9**, 336.4 g mol^{-1}): C 28.58, H 3.60, N 16.67; found: C 28.16, H 3.86, N 16.76; ^1H NMR (CD_2Cl_2): $\delta = 2.54$ ppm (s); IR (KBr): $\tilde{\nu} = 2961$ (vs), 2912 (vs), 2279 (vs), 1422 (s), 1378 (m), 1051 (m), 948 (s), 468 cm^{-1} (m).

Elemental analysis calcd (%) for $C_8H_{12}N_4Br_2Ru$ (**10**, 425.3 g mol^{-1}): C 22.60, H 2.85, N 13.18; found: C 22.73, H 2.76, N 13.45; ^1H NMR (CD_2Cl_2): $\delta = 2.54$ ppm (s); IR (KBr): $\tilde{\nu} = 2959$ (vs), 2912 (vs), 2279 (vs), 1629 (m), 1422 (m), 1045 (m), 948 (s), 517 cm^{-1} (m).

Catalysis: The precatalyst was dissolved in MeCN (20 mL). The solution was transferred into the reactor under a constant flow of argon. The desired quantities of silane **3** (2.72 g, 20.0 mmol) and CO_2 (10 g, 0.22 mol) were added at room temperature (Method A). In Method B, the reactor was heated for 15 min at 358 K with stirring the reaction mixture, before CO_2 was added. The amount of CO_2 delivered was measured by the mass difference of the CO_2 storage vessel.

The reaction mixture was stirred vigorously at 358 K at a pressure ranging between 20 and 40 bar. After depressurizing, remaining CO_2 was carefully removed by stirring at 298 K. Final conversion and selectivity were determined by ^1H NMR (D_2O insert) with a relative error of $\pm 3\%$. To confirm selectivity to formoxysilane **4**, purification was carried out for representative experiments by first removing the volatile components followed by vacuum distillation.[9a,11]

In situ FTIR spectroscopy: A multi-reflection diamond attenuated total reflection DiComp probe (ASI Applied System), connected to the ReactIR/FTIR analyzer (ASI Applied System, model 1000) through an optical conduit, was mounted in the reactor top. This allows for in situ mid-IR absorption measurements to be run in the reaction mixture. Single beam spectra comprised of 32 scans at a resolution of 2 cm^{-1} with auto gaining and Happ–Genzel apodization were collected in this analysis over the range of 4000–650 cm^{-1}. The diamond transmits IR radiation over this region excerpt for absorption regions of 2200–1900 cm^{-1} and below 650 cm^{-1}.This did not affect probe performance, as the fingerprint region (1800–650 cm^{-1}) was used to monitor catalytic hydrosilylation of CO_2. All single spectra collected during a hydrosilylation run were measured against a background spectrum in the reactor which was free from substrate. It should be noted that the background spectrum was collected by the same data collection parameters and with the same optical bench as in subsequent reaction spectra.

Quantification and calculation of reaction rates from the spectroscopic data were performed after peak height analysis. Furthermore independent measurements confirmed that, within the concentration range of interest, the intensity of absorbed infrared light was linearly proportional to the concentration of each of the reactants dissolved in MeCN. Sampling of the mixture took place along with in situ FTIR monitoring. From control samples, conversion and selectivity were determined by off-line ^1H NMR analyses.

Computational methods: All calculations presented here were performed with the Turbomole program package.[39] Because of its robustness in different chemical bonding situations, we used the DFT Becke–Perdew86 (BP86) level of theory[40] within the efficient RI–*J* approximation for the Coulomb two-electron terms.[41] For structure optimizations we employed SV(P) basis sets (single zeta for core orbitals, double zeta for valence shells and one set of polarization functions for all centers except hydrogen).[42] Single-point energies were calculated with larger triple-zeta-valence plus polarization basis sets (TZVP).[43]

Stationary points on the potential energy surface were characterized as either minima or transition states by the presence of (respectively) zero or one significantly imaginary frequency in the BP86/SV(P) vibrational spectrum, obtained by second analytic derivative calculations.[44]

In addition to (non-zero-point vibrationally corrected) potential energies, *E*, on a Born–Oppenheimer surface, we also calculated Gibbs free energies *G*: All *G* values refer to 85 °C and 30 bar CO_2 pressure. As the reaction does not take place in an ideally diluted gas phase, we modified the standard statistic thermodynamic *G* values for MeCN, Me_3SiH and the product, formoxysilane, by adding $+21.5$ kJ mol^{-1}, which corresponds to $T\Delta S_{vap}$, assuming (in a Trouton-like approach) ΔS_{vap} of all these liquids to be $+88$ kJ mol^{-1} at 1 bar and extrapolating to 30 bar. This accounts, at least in a roughly approximate way, for the fact that these compounds do not enter/leave the reaction mixture as a gas. Also, the vibrational parti-

tion function contribution to G was omitted as the calculated vibrational spectra of the complexes were found to exhibit extremely small restricted rotational frequencies for the MeCN ligands. Effects of anharmonicity and numerical accuracy, therefore, would cause straightforward application of statistic thermodynamic formulae to lead to artifacts.

To evaluate the influence of solvent effects beyond the explicitly treated first coordination sphere, other single-point energies were computed at the BP86/TZVP level of theory employing the COSMO solvation model with the dielectric constant $\varepsilon = 38$ (MeCN).[45]

Furthermore, some single-point energy calculations were also performed at the B3LYP level of theory (→B3LYP/TZVP||BP86/SV(P))[46] in order to assess how far the results obtained depend on the density functional employed.

Acknowledgements

We are grateful to the Deutsche Forschungsgemeinschaft (SFB 623, University of Heidelberg) for funding the project D5. S.P. thanks Professor E. Dinjus, Professor Dr. I. Horvath and L T. Mika for stimulating discussions and Mrs. Doreen Neumann for experimental input to the work presented.

[1] a) L. Ceyzeriat (Rhone-Poulenc), FR 1198749, **1959** [*Chem. Abstr.* **1961**, *55*, 40579]; b) L. B. Brunner (Dow Corning Corp.), US 3035016, **1962** [*Chem. Abstr.* **1963**, *59*, 82927]; c) H.-H. Moretto, M. Schulze, G. Wagner, *Silicones*, Ullmann's Encyclopedia of Industrial Chemistry, Wiley Interscience, 7th ed. **2005**, chap. 6.

[2] J. J. Packo, D. L. Bailey (Packo Industries, Inc.), US 4331722, **1982** [*Chem. Abstr.* **1982**, *97*, 25287].

[3] a) A. G. Brook, *J. Am. Chem. Soc.* **1955**, *77*, 4827; b) G. Schott, K. Deibel, *Z. Chem.* **1963**, *3*, 106; c) W. McFarlane, J. M. Seaby, *J. Chem. Soc. Perkin Trans. 2* **1972**, 1561; d) E. P. Plueddemann (Dow Corning Corp.), DE 2117028, **1972** [*Chem. Abstr.* **1972**, *76*, 14669]; e) L. Birkofer, P. Sommer, *J. Organomet. Chem.* **1975**, *99*, C1; f) M. Trommer, W. Sander, A. Patyk, *J. Am. Chem. Soc.* **1993**, *115*, 11775.

[4] a) H. Koinuma, F. Kawakami, H. Kato, H. Hirai, *J. Chem. Soc. Chem. Commun.* **1981**, 213; b) G. Süss-Fink, J. Reiner, *J. Organomet. Chem.* **1981**, *221*, C36.

[5] P. G. Jessop, *Top. Catal.* **1998**, *5*, 95.

[6] L.-N. He, J.-C. Choi, T. Sakakura, *Tetrahedron Lett.* **2001**, *42*, 2169.

[7] A. E. Mera, R. E. Morris, *Macromol. Rapid Commun.* **2001**, *22*, 513.

[8] P. Arya, J. Boyer, R. J. P. Corriu, G. F. Lanneau, M. Perrot, *J. Organomet. Chem.* **1988**, *346*, C11.

[9] a) A. Jansen, H. Görls, S. Pitter, *Organometallics* **2000**, *19*, 135; b) S. Pitter, A. Jansen, E. Dinjus (Forschungszentrum Karlsruhe GmbH), DE 19911616, **2000** [*Chem. Abstr.* **2000**, *133*, 164169].

[10] T. C. Eisenschmid, R. Eisenberg, *Organometallics* **1989**, *8*, 1822.

[11] A. Jansen, S. Pitter, *J. Mol. Catal. A* **2004**, *217*, 41.

[12] B. Marciniec, Comprehensive Handbook on Hydrosilylation, Pergamon Press, Oxford (UK), **1992**.

[13] An alternative mechanism for olefin hydrosilylation with secondary or primary silanes was proposed recently: a) P. B Glaser, T. D. Tilley, *J. Am. Chem. Soc.* **2003**, *125*, 278; b) H. Brunner, *Angew. Chem.* **2004**, *116*, 2805; *Angew. Chem. Int. Ed.* **2004**, *43*, 2749.

[14] A. J. Chalk, J. F. Harrod, *J. Am. Chem. Soc.* **1965**, *87*, 16.

[15] S. B. Duckett, R. H. Perutz, *Organometallics* **1992**, *11*, 90.

[16] P. G. Jessop, F. Joó, C.-C. Tai, *Coord. Chem. Rev.* **2004**, *248*, 2425.

[17] a) L. Appelbaum, C. Henrichs, J. Demtschuk, M. Michmann, M. Oron, H. J. Schäfer, H. Schumann, *J. Organomet. Chem.* **1999**, *592*, 240; b) C. M. Duff, G. H. Heath, *J. Chem. Soc. Dalton Trans.* **1991**, 2401; c) J. P. al Dulaimi, R. J. H. Clark, D. G. Humphrey, *J. Chem. Soc. Dalton Trans.* **2000**, 933.

[18] R. A. Sanchez-Delgado, M. Navarro, K. Lazardi, R. Atencio, M. Capparelli, F. Vargas, J. A. Urbina, A. Bouillez, A. F. Noels, D. Masi, *Inorg. Chim. Acta* **1998**, *275–276*, 528.

[19] D. E. Fogg, S. J. Rettig, B. R. James, *Can. J. Chem.* **1995**, *73*, 1084.

[20] Syntheses of complex **5**: a) N.N. (Rhone-Poulenc) GB1102460, **1968**; b) J. Dehand, J. Rose, *J. Chem. Res.* **1979**, 155; c) P. N. Komozin, *Z. Neorgan. Khim.* **2000**, *45*, 662.

[21] M. Brown, D. C. R. Hockless, *Acta Crystallogr. Sect. C* **1996**, *52*, 1105.

[22] W. E. Newton, J. E. Searles, *Inorg. Chim. Acta* **1973**, 7349.

[23] H. Endres, Comprehensive coordination chemistry, *Vol. 2* (Eds.: G. Wilkinson, R. D. Gillard, J. A. McCleverty), Pergamon Press, Oxford (UK), **1987**, p. 261.

[24] E. Ember, S. Pitter, unpublished results.

[25] The C≡N triple bond is of low reactivity towards transition metal catalyzed or promoted hydrosilylation and there are few examples known from literature: a) T. Murai, T. Sakane, S. Kato, *J. Org. Chem.* **1990**, *55*, 449; b) M. Tanabe, K. Osakada, *Organometallics* **2001**, *20*, 2118; c) H. Hashimoto, I. Aratani, C. Kabuto, M. Kira, *Organometallics* **2003**, *22*, 2199.

[26] E. W. Colvin, D. G. McGarry, *J. Chem. Soc. Chem. Commun.* **1985**, 539.

[27] S. Pitter, T. Illg, unpublished results.

[28] a) J. Li, G. Schreckenbach, T. Ziegler, *J. Am. Chem. Soc.* **1995**, *117*, 486; b) A. Görling, S. B. Trickey, P. Gisdakis, N. Rösch, *Top. Organomet. Chem.* **1999**, *4*, 109.

[29] G. I. Nikonov, *Angew. Chem.* **2001**, *113*, 3457; *Angew. Chem. Int. Ed.* **2001**, *40*, 3353.

[30] S. Lachaize, S. Sabo-Etienne, *Eur. J. Inorg. Chem.* **2006**, 2115.

[31] W. Leitner, *Coord. Chem. Rev.* **1996**, *153*, 257.

[32] A. Jansen, PhD Thesis, University of Heidelberg (**2000**).

[33] For example, $RuCl_2CO(MeCN)_3$ has absorptions for ν_{CO} at 1962 cm^{-1} and for ν_{CN} at 2280 cm^{-1}: W. E. Newton, J. E. Searles, *Inorg. Chim. Acta* **1973**, *7*, 349.

[34] A. D. Horton, A. G. Orpen, *Organometallics* **1992**, *11*, 1193.

[35] Recent examples are: a) X. Fang, J. Huhmann-Vincent, B. L. Scott, G. J. Kubas, *J. Organomet. Chem.* **2000**, *609*, 95; b) F. L. Taw, H. Mellows, P. S. White, F. J. Hollander, R. G. Bergman, M. Brookhart, D. M. Heinekey, *J. Am. Chem. Soc.* **2002**, *124*, 5100.

[36] a) M. Elder, W. A. G. Graham, D. Hall and R. Kummer, *J. Am. Chem. Soc.* **1968**, *90*, 2189; b) V. K. Bel'sky, A. N. Protsky, B. M. Bulychev and G. L. Soloveichik, *J. Organomet. Chem.* **1985**, *280*, 45; c) T. Szyman'ska-Buzar, in *Ring Opening Metathesis Polymerisation and Related Chemistry* (Eds.: E. Khosravi, T. Szyman'ska-Buzar), Kluwer Academic, Dordrecht, **2002**, pp. 349.

[37] D. Sturmayr, U. Schubert, *Eur. J. Inorg. Chem.* **2004**, 776.

[38] A. L. Osipov, S. F. Vyboishchikov, K. Y. Dorogov, L. G. Kuzmina, J. A. K. Howard, D. A. Lemenovskii, G. I. Nikonov, *Chem. Commun.* **2005**, 3349.

[39] R. Ahlrichs, M. Bär, M. Häser, C. Kölmel, *Chem. Phys. Lett.* **1989**, *162*, 165.

[40] a) S. H. Vosko, L. Wilk, M. Nusair, *Can. J. Phys.* **1980**, *58*, 1200; b) J. P. Perdew, *Phys. Rev. B* **1986**, *33*, 8822; c) A. D. Becke, *Phys. Rev. A* **1988**, *38*, 3098.

[41] a) K. Eichkorn, O. Treutler, H. Öhm, M. Häser, R. Ahlrichs, *Chem. Phys. Lett.* **1995**, *240*, 283; b) K. Eichkorn, F. Weigend, O. Treutler, R. Ahlrichs, *Theor. Chim. Acta* **1997**, *97*, 119.

[42] A. Schäfer, H. Horn, R. Ahlrichs, *J. Chem. Phys.* **1992**, *97*, 2571.

[43] A. Schäfer, C. Huber, R. Ahlrichs, *J. Chem. Phys.* **1994**, *100*, 5829.

[44] a) P. Deglmann, F. Furche, R. Ahlrichs, *Chem. Phys. Lett.* **2002**, *362*, 511; b) P. Deglmann, K. May, F. Furche, R. Ahlrichs, *Chem. Phys. Lett.* **2004**, *384*, 103.

[45] A. Klamt, G. Schüürmann, *J. Chem. Soc. Perkin Trans. 2* **1993**, *2*, 799.

[46] a) A. D. Becke, *J. Chem. Phys.* **1993**, *98*, 5648; b) C. Lee, W. Young, R. G. Parr, *Phys. Rev. B* **1998**, *73*, 785.

Received: March 21, 2006
Revised: July 8, 2006
Published online: December 19, 2006

